The Astronomical Journal, 133:1609–1614, 2007 April

EVIDENCE FOR A COLOR DEPENDENCE IN THE SIZE DISTRIBUTION OF MAIN-BELT ASTEROIDS

Paul Wiegert
Department of Physics and Astronomy, University of Western Ontario, London, ON N6A 3K7, Canada; pwiegert@uwo.ca

David Balam
Department of Physics and Astronomy, University of Victoria, Victoria, BC V8W 3P6, Canada

Andrea Moss
Department of Physics and Astronomy, University of Western Ontario, London, ON N6A 3K7, Canada

Christian Veillet
Canada-France-Hawaii Telescope Corporation, Kamuela, HI 96743, USA

and

Martin Connors and Ian Shelton
Centre for Science, Athabasca University, Athabasca, AB T6G 0R9, Canada
Received 2006 November 8; accepted 2006 December 28

ABSTRACT

We present the results of a project to detect small ($\sim$1 km) main-belt asteroids with the 3.6 m Canada-France-Hawaii Telescope. We observed in two filters (MegaPrime g' and r') in order to compare the results in each band. Owing to the observational cadence we did not observe the same asteroids through each filter and thus do not have true color information. However, strong differences in the size distributions as seen in the two filters point to a color dependence at these sizes, perhaps to be expected in this regime, in which asteroid cohesiveness begins to be dominated by physical strength and composition rather than by gravity. The best-fit slopes of the cumulative size distributions (CSDs) in both filters tend toward lower values for smaller asteroids, consistent with the results of previous studies. In addition to this trend, the size distributions seen in the two filters are distinctly different, with steeper slopes in r' than in g'. Breaking our sample up according to semimajor axis, the difference between the filters in the inner belt is found to be somewhat less pronounced than in the middle and outer belt, but the CSD of those asteroids seen in the r' filter is consistently and significantly steeper than in g' throughout. The CSD slopes also show variations with semimajor axis within a given filter, particularly in r'. We conclude that the size distribution of main-belt asteroids is likely to be color-dependent at kilometer sizes and that this dependence may vary across the belt.

Key words: minor planets, asteroids — solar system: general

1. INTRODUCTION

Observations of small (of order 1 km diameter) main-belt asteroids (MBAs) present a considerable challenge. As a result, this faint (typically $V \geq 22$) population of asteroids has not been sampled as well as it might be. The asteroid size distribution in the main belt is affected by a number of factors, the most important of which is thought to be collisions with other asteroids. It is well known that if the bodies are uniform in composition and respond to collisions in a size-independent way (i.e., have the same strength-to-mass ratio), the differential size distribution in a steady state is independent of the details of the collisions and is given by a power law:

$$dN \propto D^{-p}\, dD, \tag{1}$$

where D is the diameter, dN is the number of bodies in the size range D to $D + dD$, and the index $p = 3.5$ (Dohnanyi 1969).

This description is an idealization: in reality, asteroids are affected by size-dependent phenomena (e.g., the Yarkovsky effect, size-dependent internal strength) and are not in a true steady state (bodies are occasionally broken up and inevitably ground down to smaller and smaller sizes, and material also leaves the belt through orbital resonances). It is expected rather that the main belt will show a depletion of bodies at smaller sizes, which have less gravitational reinforcement than larger bodies and are hence more fragile per unit mass, as well as being more quickly removed by Yarkovsky forces, and that the ideally featureless power-law slope may display "waves" as a result of these removal processes (Davis et al. 1994; Durda et al. 1998; O'Brien & Greenberg 2003).

In this paper the size distribution of the main belt at kilometer to subkilometer sizes is measured in two filters, in order to extend our knowledge into the regime ($D \lesssim 1$ km) in which internal strength plays an increasingly important role in the bodies' responses to collisions (Farinella et al. 1982; Housen & Holsapple 1990, 1999; Benz & Asphaug 1999), and in which compositional differences (possibly indicated by color differences) become increasingly important to asteroid cohesiveness and strength.

2. OBSERVATIONS AND DATA REDUCTION

All images were taken with the MegaPrime MegaCam on the 3.6 m Canada-France-Hawaii Telescope (CFHT) atop Mauna Kea in Hawaii. MegaCam uses 40 2048×4612 pixel CCDs, covering a $1^\circ \times 1^\circ$ field of view with a resolution of $0.187''$ pixel^{-1}. The images used were taken as part of the "Very Wide" (VW) segment of the CFHT Legacy Survey (CFHTLS). Seven sets of observations were taken in the MegaPrime g' filter ($\sim$400–580 nm) on either 2004 December 15–16 or 2005 January 16–17, and 19 sets in the MegaPrime r' filter ($\sim$550–700 nm) were taken on the nights of 2006 May 1– 2 and May 25–26.

Images from the VW segment of the survey were chosen for this study because of its cadence: three images were taken of the

same field at approximately 45 minute intervals during the course of the first night, followed by a single image of the same field the following night. The large field of view of the camera means that (1) many asteroids are seen in any given frame and (2) many of these can be followed up successfully on the second night, which allows for somewhat improved orbits and geocentric and heliocentric distances, and hence sizes.

Data were obtained in both the MegaPrime g' and r' filters in order to compare results at two wavelength ranges. The CFHTLS VW segment also acquired images in the i' filter. However, these were taken far from opposition. As a result, it proved much more difficult to make accurate heliocentric and geocentric distance determinations (even given a detection on the second night), and we excluded them from our sample.

The exposure times were 90 s in g' and 110 s in r'. Seeing sizes were 0.8″ and 1.1″, respectively, for the two dates on which the g' frames were taken. The limiting magnitude for a 50% probability of a 3 σ detection on the g' frame with 1.1″ seeing was 23.0, and the 90% probability limit was 22.5. For the r' frames the seeing was 1.0″ and 1.1″ for the two dates, and the limiting magnitude for a 3 σ detection was 21.75 and 22.25 for 90% and 50%, respectively, for the night with the worse seeing. The limiting magnitude was determined by calibrating a set of images containing artificially implanted sources moving at rates consistent with those of MBAs. The images used for the seeding were real data images from the CFHTLS; the artificial sources were implanted using the `mkobjects` function of IRAF (Tody 1986). The information was used to set a detection limit, which we chose to be 90% completion (that is, 21.75 in r' and 22.5 in g'). We based our further analysis only on those objects brighter than the above limits.

The CFHTLS images were processed by the Elixir pipeline (Magnier & Cuillandre 2004), which includes bias and dark subtraction, flat-fielding, and fringe subtraction. Photometric corrections including color terms were computed at this time. The images were then processed by the TERAPIX data-processing center based in Paris for fine astrometric correction to the USNO-B1.0 catalog (Monet et al. 2003). The cleaned images were stored at the Canadian Astronomical Data Centre, from which we retrieved them and began the search for moving objects.

The fields in the different filters were taken at different times. No attempt was made to take images in both filters on the same night, nor to follow particular asteroids for more than two nights. As a result, the fields taken with different filters do not contain the same asteroids (except possibly by chance). Thus, the size distributions determined in the g' and r' filters are for two statistically similar samples of asteroids rather than for the same sample as seen through the two filters. The total survey areas were seven fields ($\sim$7 deg^2) in the g' band and 19 fields ($\sim$19 deg^2) in the r' band, with all fields taken within $\pm 2^\circ$ of the ecliptic.

2.1. *Asteroid Detection*

In order to detect MBAs in our images, the software package Source Extractor (Bertin & Arnouts 1996) was used to build a catalog of all sources more than 3 σ above the background and provide the sources' positions (both [x, y] and [R.A., decl.]), magnitudes, and full widths at half-maximum, as well as flags that described sources that were saturated, truncated, blended with another, or located on bad pixels. The earlier TERAPIX processing of the frames produced photometric corrections for filter and air mass, and these were applied by Source Extractor in the calculation of the magnitudes.

Stationary objects were then removed, as were sources with the obvious characteristics of cosmic rays. The remaining sources were then searched for triplets moving within the appropriate range of angular rates. Those detected were considered candidate one-night asteroid detections.

The image areas surrounding each candidate were then blinked, and a human operator determined whether the candidate was real or the result of imperfect cosmic-ray removal, variations in the image quality during the night, or other causes. Candidates not clearly visible and asteroidal in appearance in all three frames were discarded. Those that remained constituted our sample of one-night objects and were subjected to further analysis, both as to their size distribution and as to whether or not they were seen on the second night's image.

In order to determine whether or not an object appeared in the second night's image, the motion of the candidate was extrapolated linearly forward in time. If the position was determined to have moved out of the field of view, the processing proceeded no further. If it was predicted to fall within the second night's image, a blink frame of the section of the second night's image around the predicted position was compared to the same region taken the previous night. If blinking revealed an object of appropriate magnitude near the appropriate location on the second night, the object was deemed to have been detected on the second night. A final consistency check was performed by computing an orbit for the object based on the two nights of observations, and verifying that the motion was reasonable and within the main belt (Trojan asteroids, Centaurs, and Kuiper Belt objects were occasionally picked up). The final catalog of one- and two-night detections was analyzed for its size-frequency distribution.

We saw 686 main-belt objects on only a single night, and 839 on two nights, or 272 (414) and 245 (594) one- and two-night objects, respectively, in the g' (r') filters. A total of 1525 asteroids were detected, at a rate of 73 and 53 asteroids deg^{-2} in the g' and r' filters, respectively.

2.2. *Orbital Elements*

For the single-night detections, the observed arc was approximately 1.5 hr long. In order to compute the semimajor axis and inclination, we used Väisälä's method (Väisälä [1939] as described in Dubyago [1961]) based on the assumption that one observation was taken at perihelion. A method proposed by Dubyago in that same work and based on the assumption of a circular orbit was also tested. Comparisons done using known asteroids with well-determined orbits revealed Väisälä's method to be somewhat superior for these objects with very short arcs. For the two-night detections, Herget's method (as described in Danby 1989) was used because of its slightly superior performance when tested on observations of known asteroids. Herget's method requires estimates of the geocentric distance of the body in question; however, these can be obtained fairly accurately given observational arcs of about 1 day for asteroids within the main belt.

2.3. *Absolute Magnitudes and Diameters*

The absolute magnitude H_k in filter k is determined from the apparent magnitude m_k from

$$m_k = H_k + 5 \log (r\Delta) + P(\alpha), \quad (2)$$

where r and Δ are the heliocentric and geocentric distances of the asteroid, α is the phase angle, and $P(\alpha)$ is the phase function. We use $P(\alpha)$ from Bowell et al. (1989) with a G of 0.15. In all cases the phase angle is small, ranging from 1.7° to 7.0°, with a mean of 3.9°. The rms errors in r and Δ (which are strongly correlated and essentially equal in our sample) were both 0.38 and 0.32 AU for the one- and two-night detections, respectively. We had hoped that the two-night observations would provide us with significantly

improved accuracy in r and Δ. However, a longer arc, of order a week, is likely required to achieve much improvement. Errors in m_k were relatively small, and as a result errors in H_k (0.69 or 0.54 mag for the one- and two-night detections, respectively) are dominated by the uncertainties in r and Δ.

The diameter estimate is derived from Bowell et al. (1989),

$$D = \frac{1347 \times 10^{-H_k/5}}{A_k^{1/2}}, \quad (3)$$

where D is the diameter in kilometers and A_k is the albedo in filter k. The uncertainty in D receives nearly equal contributions from the albedo and H_k: the 1 σ error is 0.4 or 0.36 km for the one- or two-night detections.

The cumulative number distribution for MBAs brighter than an absolute magnitude H_k (i.e., having a magnitude less than H_k) can be approximated as

$$\log N(<H_k) = C + \gamma H_k, \quad (4)$$

where N is the cumulative number of asteroids and γ and C are constants, with γ being the slope. Rewriting the equation above in terms of diameter yields

$$N(>D) \propto D^{-b}. \quad (5)$$

Here, the power-law index b corresponds to the slope of the $\log N$ versus $\log D$ plot, and is connected to the constant γ by $b = 5\gamma$. Using the method of Yoshida et al. (2003), we use b to express the slope of the cumulative size distribution (CSD) of asteroids. Note that the slope of the size-frequency distribution is expressed in a variety of ways in the literature; a useful "translation table" can be found in Appendix A of O'Brien & Greenberg (2005).

2.4. *Previous Work*

There are a few major surveys that have calculated CSD slopes to which we can compare our own value. The first is the Yerkes-McDonald Survey, which was the first (1951–1952) systematic photographic survey with asteroid magnitudes based on a photometric system. They found 1550 asteroids with a limiting magnitude of 16.5. They calculated a CSD slope of $b = 2.4$ for asteroids from 30 to 300 km (Kuiper et al. 1958). The next major survey, Palomar-Leiden, was another photographic survey, performed in 1960, and extended the magnitude-frequency distribution to a magnitude of about 20. They found over 2000 asteroids and calculated a slope of $b = 1.8$ for asteroids larger than 5 km in diameter (van Houten et al. 1970).

From 1992 to 1995 Spacewatch detected 59,226 asteroids larger than 5 km. The limiting magnitude for this survey was about 21 in the visual band and yielded a CSD slope again of $b = 1.8$ (Jedicke & Metcalfe 1998). A survey of a relatively small field (15′ square) by the *Infrared Space Observatory* at 12 μm saw 20 sources and deduced a shallow slope for smaller asteroids as well, in this case $b = 1.5$ (Tedesco & Desert 2002). A study of asteroid sizes performed with archived frames from the *Hubble Space Telescope* WFPC2 taken from 1994 to 1996 revealed 96 moving objects with apparent magnitudes down to 24, or with diameters of 0.3–3 km (Evans et al. 1998). This work found a slope of 1.2–1.3, even shallower than that found by previous investigators.

The Sloan Digital Sky Survey, carried out between 1998 and 2000, systematically mapped an enormous part of the sky and produced detailed images allowing the determination of positions and absolute magnitudes of many celestial bodies, including many asteroids. Ivezič et al. (2001) used this survey to calculate a CSD slope for 13,000 asteroids down to a magnitude of 21.5 (in the R-band filter) and obtained a value of $b = 1.3$ for asteroids in the diameter range 0.4–5 km. The Sub-km Main-Belt Asteroid Survey performed at the Subaru telescope found 1111 asteroids down to a limiting magnitude of 24.4 and calculated the CSD for asteroids between 0.5 and 1.0 km to have $b = 1.2$ (Yoshida et al. 2003). However, not all studies have revealed a shallowing slope at smaller sizes. A recent report gives a constant $b = 1.9$ slope down to roughly 23 mag in V (Davis et al. 2006).

Most studies have reported that subkilometer asteroids display a somewhat shallower CSD slope than the largest ones: this implies a deficit in the smaller asteroids, indicative of some changing physics as we move into the regime in which collisional fragmentation becomes more dependent on internal strength and less on gravity.

3. RESULTS

The cumulative distributions of asteroid diameters in our sample are shown in Figure 1, with the assumption that all asteroids have an albedo of 0.09. The shaded region below each observed distribution indicates the difference between the observed CSD (*thick line*) and that which only includes asteroids brighter than our 90% completion limit. Thus, the thickness of the shaded region gives us a measure of how much our sample is affected by incompleteness. In fitting slopes to the observed distribution, we only use those points for which the shaded area is less than 10% of the height of the observed distribution. Put another way, we only fit those points for which objects fainter than our completeness limit contribute less than 10% to the height of the distribution at a given point, to eliminate a skewing of the distribution due to incompleteness.

The error bars on the CSDs are determined by a standard bootstrap process (Efron 1982). Using our sample of diameter measurements, each with an individually computed uncertainty, we generated 100 statistically similar distributions by a Monte Carlo process under the assumption that the errors are distributed in a Gaussian fashion. The plotted error bars in the figures represent 1 standard deviation as computed by the bootstrap process at each point.

The least-squares lines shown in the figures are fitted only to data points for which the observed CSD and that based on the 90% completion limit differ by less than 10%. The data points are weighted by $1/\sigma$ during this fit to properly account for the larger error bars in the larger diameter region of the plot, although an unweighted fit produces similar results. We note, however, that the distributions do not seem particularly well fitted by a straight line in this range; there are features that deviate from the line by more than the height of the error bars in Figure 1. Deviations from a pure power-law slope for asteroid CSDs are now well known and have been discussed by many authors, for example, Cellino et al. (1991), Durda & Dermott (1997), Durda et al. (1998), and O'Brien & Greenberg (2003).

The difference between the slopes in the two filters is quite clear in Figure 1. The best-fit slope for the g' sample is $b = 1.87 \pm 0.05$, while that for the r' filter is $b = 2.45 \pm 0.07$. We also note that the slope difference is not simply due to our relatively fine binning. A coarser binning, shown in Figure 2, produces least-squares fit slopes that show the same trend (1.94 ± 0.15 and 2.23 ± 0.11). The difference in the slopes is not quite as distinct and has larger uncertainties, as we are fitting the line to

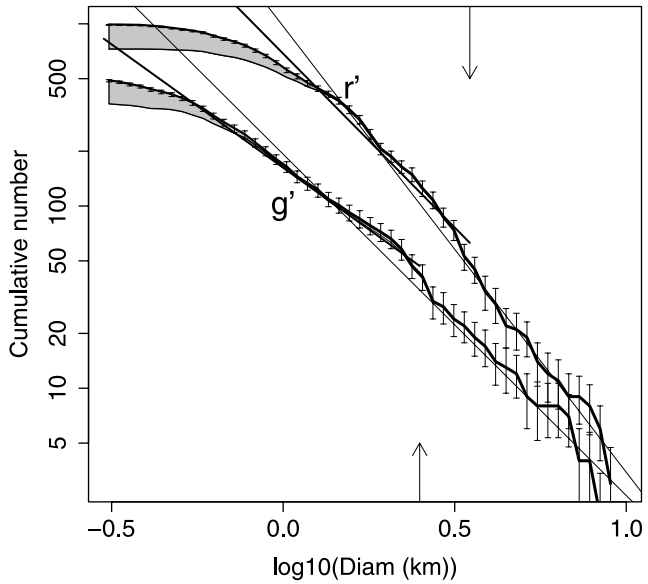

FIG. 1.—CSDs of MBAs as detected in the r' and g' filters (*thick lines*). The shaded areas indicate the difference between the observed distributions and those in which we exclude all objects whose apparent magnitude is below our 90% completeness limit. The straight lines are the weighted least-squares fit slopes to the size distributions, including only those points for which our completeness is above 90%. The locations of the slope changes at diameters of ~2.5 (g') and ~3.5 (r') km are indicated by the arrows (see text). The thick line segments extending to the left of the knees are the best-fit slopes for these smaller asteroids.

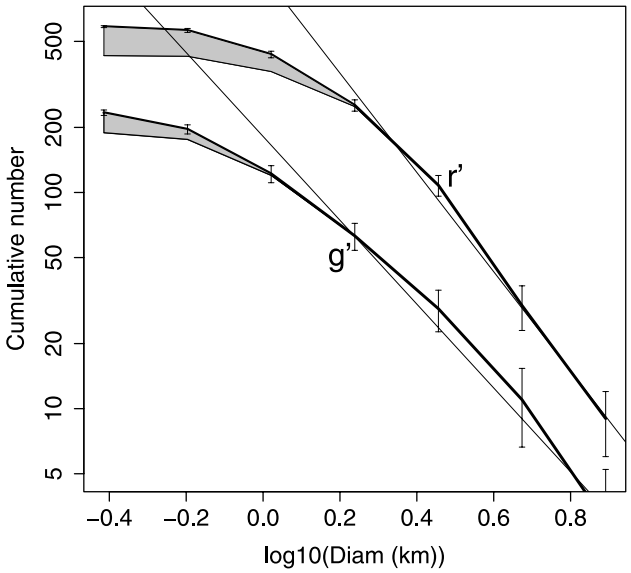

FIG. 2.—CSD with larger bin sizes.

relatively few points (we continue to exclude those beyond our 90% completeness limits), yet the slopes still differ by about 2 σ.

Before discussing the difference between the g' and r' slopes, we remind the reader that both are calculated using the same assumed albedo of 0.09. Both samples show evidence for at least one change in the power-law slope, at roughly 2.5 km in g' and 3.5 km in r' (see Fig. 1). The location of this change in the slope, or "knee," corresponds roughly to that seen in other determinations of the CSD, for example, that in Figure 1 of O'Brien & Greenberg (2005). The causes of such deviations of the asteroid size distribution from a smooth power law remain under study, but almost certainly reflect the influence of size-dependent processes in the asteroid belt.

A slope calculated only from asteroids smaller than this knee yields values of $b = 1.35 \pm 0.02$ and 1.79 ± 0.07 in the visible and red, respectively, shallower than the overall slope in each case. Owing to the small number of asteroids larger than the knee in our sample, we did not calculate the slope for these bodies on their own. Their effect on the slope when excluded from the least-squares fit is sufficient to show their tendency toward a steeper slope than for the smaller asteroids. Thus, both filters show a reduced slope for smaller bodies, which is consistent with other observational results in which, despite variations, a general trend toward shallower slopes at smaller diameters is evident. This trend has been associated with size-dependent depletion of small asteroids because (1) they may acquire higher velocities during collisions (Petit & Farinella 1993; Campo Bagatin et al. 1994), (2) they are subject to larger Yarkovsky drifts (Bottke et al. 2000), and (3) they have lower strengths per unit mass (Farinella et al. 1982; Housen & Holsapple 1990, 1999; Benz & Asphaug 1999).

Our interpretation of why our results show slopes generally steeper than those reported earlier at these sizes is simply that a single power law is not a very good fit to the size distribution of the entire belt. We have examined a relatively narrow size range (only about 1 and a half orders of magnitude in diameter). This is roughly the size of the "waves" expected in the distribution due to size-dependent processes (see Fig. 6 in Durda & Dermott 1997).

Of more interest are the differing CSD slopes for asteroids viewed in different filters, although such a difference is perhaps not unexpected. As one moves toward smaller sizes, strength becomes composition-dependent as gravity becomes less of a factor, and it is known that there are widely differing compositions in the asteroid belt. Simply speaking, each sample should contain different proportions of asteroids with different colors, and hence compositions and internal properties. Since internal properties are important to the bodies' strengths at these sizes, the collisionally induced size distribution might be expected to be different. An alternative explanation is that there is a single population of asteroids, but that there is a trend toward increasing redness for smaller and smaller asteroids. Since we have assumed a fixed albedo in both filters, this color trend would skew the slope of the red CSD to a larger value. More information will be required to distinguish between these and other alternative explanations of the observations.

We are not aware of a color or filter dependence in the size distribution having been reported before. This might be explained by the relatively few earlier studies that could reach this size range or, in the cases of those that did, by an absence of color information.

In order to examine the difference in slope with filter more extensively, we split our sample into three semimajor axis regions, following Yoshida & Nakamura (2004). The three zones used are the inner (2.0 AU $< a \leq$ 2.6 AU), middle (2.6 AU $< a \leq$ 3.0 AU), and outer (3.0 AU $< a \leq$ 3.5 AU) zones. Our semimajor axis determination has an uncertainty of $\pm$0.3 AU based on the comparison of our calculations with known asteroids (observed by chance), so this division is a rough one but helps reveal whether the different slopes remain evident in subsamples of our data set. The diameter distributions for each region are shown in Figures 3, 4, and 5.

In these subsamples the slope differences between filters persist, with the red slope consistently steeper in each subsample. However, the slopes are not constant across the belt in either filter.

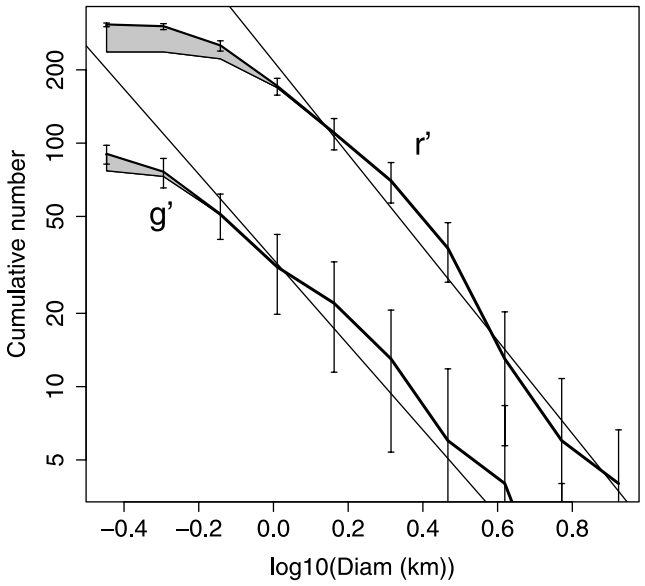

FIG. 3.—Diameter distribution for the inner section of the belt (2 AU $< a <$ 2.6 AU).

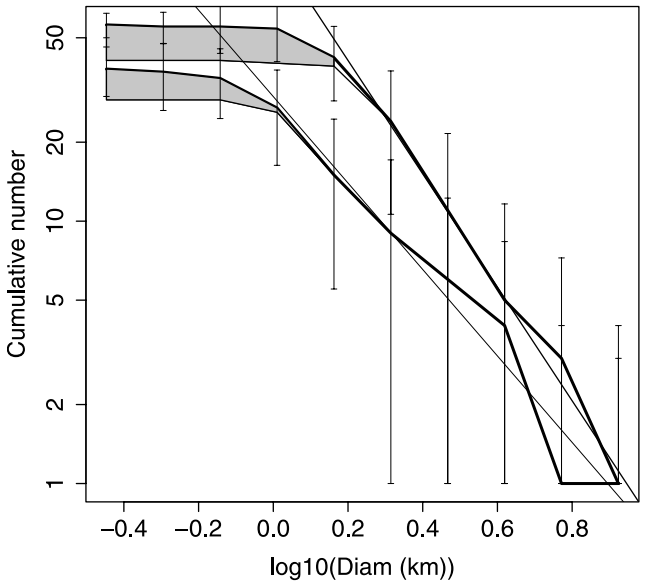

FIG. 5.—Diameter distribution for the outer section of the belt (3.0 AU $< a <$ 3.5 AU).

The slope of the r' distribution shows strong variations with semimajor axis (see Table 1). The least-squares fit for the middle region (Fig. 4) has the steepest slope ($b = 2.39 \pm 0.07$), with the outer region (Fig. 5) next ($b = 2.25 \pm 0.08$). The inner region (Fig. 3) has the shallowest slope in r' ($b = 2.00 \pm 0.05$). The g' distributions have a less dramatic but similar trend, also showing the steepest slope in the middle belt ($b = 1.85 \pm 0.06$), while the inner and outer belts are similar at $b = 1.58 \pm 0.06$ and 1.60 ± 0.07, respectively. These differences across the asteroid belt may be due to the well-known compositional variations with semimajor axis (Gradie & Tedesco 1982; Mothé-Diniz et al. 2003).

In order to examine these findings in more detail, we also compute the slope for those asteroids with sizes smaller than the knee mentioned earlier. This allows us to work in a region where the error bars are smaller, and puts us more firmly in the regime in which strength depends more on internal composition, and thus in which color-related effects may be stronger. Although we would expect the absolute slopes of these smaller diameter sections of the distributions to be shallower (as discussed earlier in this section), they can be examined to see whether they show the same trends.

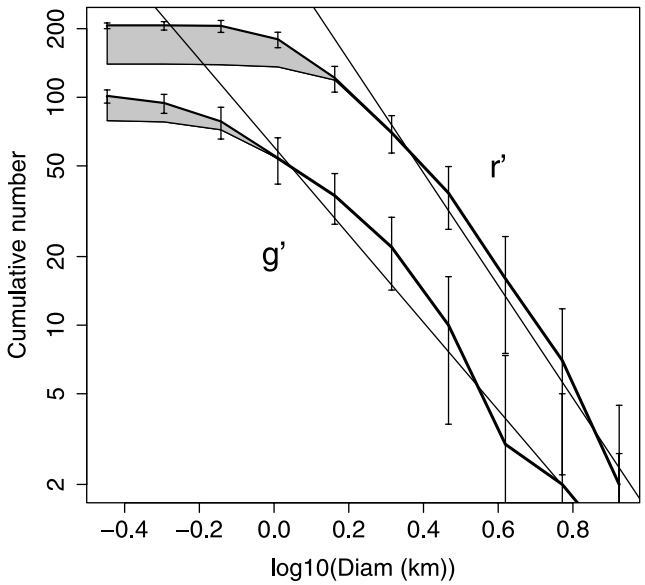

FIG. 4.—Diameter distribution for the middle section of the belt (2.6 AU $< a <$ 3.0 AU).

These more finely divided subsamples show the same qualitative behavior seen in the larger samples. Both (1) the significantly higher slope in the red versus the visible across the belt and (2) higher slopes in r' in the middle/outer belt are seen. The results are summarized in Table 2. An overall shallower slope at these smaller sizes, expected from our examination of the complete samples, is seen, but the filter-related differences persist. There are other small differences, the main one being that the slopes of these subsamples in r' in the middle and outer belts are equal ($b = 1.8 \pm 0.07$ and 1.81 ± 0.09; Table 2), whereas they differ in the complete sample ($b = 2.39 \pm 0.07$ and 2.25 ± 0.08; Table 1). However, the outer region is where we have the fewest objects, and hence is likely to be the least reliable in terms of slope determination.

Thus, we conclude that there is a real difference in the slopes of the CSDs as seen in the two filters, and that this difference appears strongest in the middle and outer asteroid belt but somewhat less pronounced in the inner belt. The slope of the CSD in the g' filter shows weak variations throughout the belt, while the r'

TABLE 1

FILTER DEPENDENCE OF THE SLOPE OF THE SIZE DISTRIBUTION

Filter	Range	b	N
g'	All	1.87 ± 0.05	185
r'	All	2.44 ± 0.07	423
g'	Inner	1.58 ± 0.06	77
r'	Inner	2.00 ± 0.05	238
g'	Middle	1.85 ± 0.06	79
r'	Middle	2.39 ± 0.07	143
g'	Outer	1.60 ± 0.07	29
r'	Outer	2.25 ± 0.08	42

TABLE 2
Filter Dependence of the Slope of the Size Distribution of the Smallest Asteroids

Filter	Range	b	N
g'	All	1.35 ± 0.02	167
r'	All	1.91 ± 0.08	384
g'	Inner	1.20 ± 0.03	71
r'	Inner	1.58 ± 0.06	224
g'	Middle	1.39 ± 0.07	73
r'	Middle	1.80 ± 0.07	124
g'	Outer	1.31 ± 0.05	23
r'	Outer	1.81 ± 0.09	36

distribution shows larger changes, particularly from the inner to the middle/outer belt. The persistence of the slope differences when the sample is subdivided gives us some confidence that the result is real. At the very least, it seems likely that the asteroid size distribution is color-dependent within certain regions of the main belt and that this color dependence changes across the belt.

A number of different scenarios could be imagined as causes for the slope differences across the belt, most tied to the known composition gradient across the main belt. C types predominate in the outer belt, while S types are more abundant in the inner belt (Gradie & Tedesco 1982), although later studies differ somewhat on the distance at which the transition takes place (Mothé-Diniz et al. 2003). Given as well that C types are redder than S types over the wavelength range we examine here (see, e.g., Gaffey et al. 1993), this could indicate that we are seeing differences associated with compositional variations across the belt. However, despite the temptation to link the samples as seen through the different filters with particular asteroid types, it is clear that we do not have enough information to make unique associations. We cannot distinguish between the effects of color, albedo, size, age, and strength in this system, making a determination of the cause of the different slopes a difficult task. We do not have true color information on any asteroids observed, as none of the bodies were seen through both filters, nor do we have albedos. One could imagine an age-dependent component as well, as small asteroids are statistically younger and because asteroid weathering produces redder colors but is not expected to affect C- and S-type asteroids equally. More observations and better spectral coverage are required to determine the cause of the color dependence on size across the main asteroid belt.

4. CONCLUSIONS

We detected 517 and 1008 main-belt asteroids in the g' and r' filters, respectively, in CFHTLS MegaPrime MegaCam images. A general trend toward shallower slopes in the CSD was found as one moves toward smaller diameters, as has typically been found by other researchers. Our overall best-fit slopes are typically higher than reported previously, which we attribute to the sensitivity of the slope determination to deviations from a pure power law and to the narrow range of diameters in our sample. We determine that the overall size distribution does show a filter dependence over the size range examined, indicating that smaller asteroids in the sample seen in the r' filter are relatively more abundant than those we detect in g'. This difference is weaker in the inner belt but prominent in the middle and outer parts of the belt. We conclude that there is evidence for a color dependence in the size distribution of asteroids in the 0.3–10 km diameter range, a variation whose strength differs across the belt, although further investigation is required to determine the underlying causes of the observed differences.

We thank Richard Greenberg for insightful comments that substantially improved this manuscript. This research was performed in part with support from the National Science and Engineering Research Council of Canada. This work is based on observations obtained with the MegaPrime MegaCam, a joint project of CFHT and CEA/DAPNIA, at the Canada-France-Hawaii Telescope, which is operated by the National Research Council (NRC) of Canada, the Institut National des Sciences de l'Univers of the Centre National de la Recherche Scientifique (CNRS) of France, and the University of Hawaii. This work is based in part on data products produced at TERAPIX and the Canadian Astronomy Data Centre as part of the CFHT Legacy Survey, a collaborative project of the NRC and CNRS. This research used the facilities of the Canadian Astronomy Data Centre operated by the NRC of Canada with the support of the Canadian Space Agency.

REFERENCES

Benz, W., & Asphaug, E. 1999, Icarus, 142, 5
Bertin, E., & Arnouts, S. 1996, A&AS, 117, 393
Bottke, W. F., Jr., Rubincam, D. P., & Burns, J. A. 2000, Icarus, 145, 301
Bowell, E., Hapke, B., Domingue, D., Lumme, K., Peltoniemi, J., & Harris, A. 1989, in Asteroids II, ed. R. Binzel, T. Gehrels, & M. Matthews (Tucson: Univ. Arizona Press), 524
Campo Bagatin, A., Farinella, P., & Petit, J.-M. 1994, Planet. Space Sci., 42, 1099
Cellino, A., Zappala, V., & Farinella, P. 1991, MNRAS, 253, 561
Danby, J. M. A. 1989, Fundamentals of Celestial Mechanics (Richmond: Willmann-Bell)
Davis, D. R., Gladman, B., Jedicke, R., & Williams, G. 2006, AAS DPS Meeting, 38, 53.01
Davis, D. R., Ryan, E. V., & Farinella, P. 1994, Planet. Space Sci., 42, 599
Dohnanyi, J. S. 1969, J. Geophys. Res., 74, 2531
Dubyago, A. D. 1961, The Determination of Orbits (New York: MacMillan)
Durda, D. D., & Dermott, S. F. 1997, Icarus, 130, 140
Durda, D. D., Greenberg, R., & Jedicke, R. 1998, Icarus, 135, 431
Efron, B. 1982, The Jackknife, the Bootstrap, and Other Resampling Plans (Philadelphia: Soc. Ind. Appl. Math.)
Evans, R. W., et al. 1998, Icarus, 131, 261
Farinella, P., Paolicchi, P., & Zappala, V. 1982, Icarus, 52, 409
Gaffey, M. J., Burbine, T. H., & Binzel, R. P. 1993, Meteoritics, 28, 161
Gradie, J., & Tedesco, E. 1982, Science, 216, 1405
Housen, K. R., & Holsapple, K. A. 1990, Icarus, 84, 226
———. 1999, Icarus, 142, 21
Ivezič, Ž., et al. 2001, AJ, 122, 2749
Jedicke, R., & Metcalfe, T. S. 1998, Icarus, 131, 245
Kuiper, G. P., Fugita, Y. F., Gehrels, T., Groeneveld, I., Kent, J., van Biesbroeck, G., & van Houten, C. J. 1958, ApJS, 3, 289
Magnier, E. A., & Cuillandre, J.-C. 2004, PASP, 116, 449
Monet, D. G., et al. 2003, AJ, 125, 984
Mothé-Diniz, T., Carvano, J. M. Á., & Lazzaro, D. 2003, Icarus, 162, 10
O'Brien, D. P., & Greenberg, R. 2003, Icarus, 164, 334
———. 2005, Icarus, 178, 179
Petit, J.-M., & Farinella, P. 1993, Celest. Mech. Dyn. Astron., 57, 1
Tedesco, E. F., & Desert, F.-X. 2002, AJ, 123, 2070
Tody, D. 1986, Proc. SPIE, 627, 733
Väisälä, Y. 1939, Astron.-Opt. Inst. Univ. Turku Informo, 1, 32
van Houten, C. J., van Houten-Groeneveld, I., Herget, P., & Gehrels, T. 1970, A&AS, 2, 339
Yoshida, F., & Nakamura, T. 2004, Adv. Space Res., 33, 1543
Yoshida, F., Nakamura, T., Watanabe, J.-I., Kinoshita, D., Yamamoto, N., & Fuse, T. 2003, PASJ, 55, 701